Bol. Soc. Paran. Mat.
©SPM – E-ISSN-2175-1188
SPM: www.spm.uem.br/bspm

(3s.) **v. 2025 (43) 3** : 1–13.
ISSN-0037-8712
doi:10.5269/bspm.79158

Influence of Anisotropic Permeability on Brinkman-Darcy-Forchheimer Flow Through Curved Channels

V. K. Narla and R. Vijaya Sree* and K. Suresh Babu

ABSTRACT: The analysis of fluid motion in curved channels embedded with porous structures is important for understanding transport phenomena in complex geometries. The study examines the steady, laminar flow of an incompressible fluid through a curved channel saturated with an anisotropic porous medium, highlighting the combined effects of channel curvature and directional permeability. The flow is generated by an azimuthal pressure gradient. The Brinkman–extended Darcy–Forchheimer model, which accounts for viscous shear, Darcy resistance, and inertial Forchheimer effects, is used to formulate the governing equations, which are solved numerically by using the spectral quasilinearization method (SQLM). An internal MATLAB program was employed to generate velocity and temperature profiles for various physical parameters. The analysis shows that increasing the anisotropic permeability ratio from $K = 0.5$ to $K = 2$ reduces peak velocity by 33% and raises central temperature by 28%. Similarly, as the channel transitions from a highly curved state from $\kappa = 1.25$ to $\kappa \to \infty$, peak velocity decreases by 70% and central temperature increases by 16%, reflecting the reduced influence of centrifugal forces. Unlike isotropic models, this work quantifies how anisotropy and non-Darcy effects interact with curvature, offering predictive insights for porous flow systems, biomedical devices, and heat exchangers.

Key Words: Curved channels, anisotropic permeability, porous media, Brinkman-Darcy-Forchheimer model.

Contents

1. Introduction

Analysis of fluid movement in curved channels is essential for enhancing several applications, including industrial heat exchangers, piping systems, biomedical devices, and natural systems such as rivers and blood passages. When fluid channels are curved, they exhibit distinct flow properties, including secondary flows, increased mixing, and modified pressure and velocity distributions. This makes curved channels efficient in enhancing heat and mass transfer, fluid mixing, and system stability. Comprehending these flow dynamics enables engineers and scientists to create extremely efficient, long-lasting, and operational systems in many fields. The curvilinear coordinate system for curved channel flow was first introduced by Goldstein [1]. Accordingly, R.M. So [2] used Goldstein's curvilinear coordinate system to approximate the entry flow in a curved channel. From this investigation, it was concluded that the wall curvature leads to an increase in the entrance region length. It also revealed that the curvature of the wall had an impact on pressure drop along both the inner and outer walls. Initially, scientists and researchers worked on the fluid flow through simple geometries. Subsequently, practical applications necessitate the investigation of fluid flow through complex geometries occupied by porous media. A porous medium is a material that contains interconnected voids or pores within its solid matrix. Such materials are characterised primarily by two properties: porosity and permeability. Porosity represents the fraction of void volume to the total

* Corresponding author.
2010 *Mathematics Subject Classification:* 76M25, 76S05.
Submitted September 25, 2025. Published October 16, 2025

volume of the material, while permeability measures the ease with which a fluid can pass through the porous structure.

The study of fluid flow in porous media has numerous applications, including oil recovery, blood flow through arteries, nuclear reactor cooling, and various filtration and biomedical processes. Some studies which examined fluid flow in porous conduits can be found in literature [3]–[10]. Berman [11] studied the fluid flow through a porous channel. The permeability of the material and the size of the channel under consideration were found to affect the constant permeation rate in this study. Kuznetsov and Avramenko [12] investigated laminar flow in a curved channel with a rectangular cross-section filled with porous material, employing the Brinkman-extended Darcy law. By applying the Fourier series, a solution was obtained analytically for the velocity field. A correlation was demonstrated between the velocity distribution and the channel geometry as well as the Darcy number. Okechi and Asghar [13], in their study, examined the viscous fluid's flow along a porous curved and corrugated channel. A Darcy Brinkman model was employed to characterise fluid flow, analysing the impacts of channel curvature, wall corrugations, and medium permeability on flow within a porous medium. Yadav and Yadav [14] investigated the properties of couple stress fluid flow in a curved channel, considering a porous medium. The findings showed that porous medium's permeability and channel curvature had a considerable impact on the overall efficiency of heat transfer. For solving the system of equations that governs the flow, the Homotopy Analysis Method was employed.

The consideration of anisotropy in porous media further complicates the flow, and some studies that examined the effect of anisotropy on fluid dynamics can be found in [15]–[20]. Karmakar and Raja Sekhar [21] conducted an analysis on the impact of anisotropic parameters on fluid flowing along two porous channels. The modelling of the flow of fluids in curved channels with anisotropic permeability poses a highly complex scenario. Exploring the fluid flows in curved anisotropic porous conduits was motivated by a multitude of practical applications. As an example, in the field of biomedical engineering, curved channels are commonly found in biological systems like blood vessels. These systems are often anisotropic because of the diverse structure of tissues. Moreover, industrial applications involving filtration and separation systems can benefit from optimised designs that consider both anisotropy and channel curvature.

Previous studies have largely neglected the combined effects of curvature and anisotropy in porous channel flows. While individual aspects have been addressed, such as curvature or anisotropy by Karmakar and Raja Sekhar [22] and anisotropy by Nakayama et al. [23], an integrated investigation of both phenomena has remained limited. Recent studies have extensively explored fluid flow and heat transfer in curved and porous geometries with various enhancements. For instance, the mixed convective flow of Ag–H_2O magnetic nanofluid over a curved surface with volumetric heat generation and temperature-dependent viscosity has been analysed to understand the interplay of buoyancy and thermophysical effects [24]. The impact of anisotropic slip on magnetised tangent hyperbolic fluid flow over a rotating disk was investigated using the Legendre wavelet collocation method, highlighting the role of slip and non-Newtonian behaviour in modifying flow and heat transfer [25]. Darcy–Forchheimer flow of CNTs–H_2O nanofluid over a porous stretchable surface using the Xue model provided insights into non-Darcy resistance and nanofluid enhancement [26]. Additionally, melting heat transfer and irreversibility analysis in Darcy–Forchheimer flow of Casson fluid modulated by EMHD over cone and wedge surfaces emphasised the significance of thermal gradients and magnetic effects on entropy generation [27]. Motivated by these findings, the present study investigates the combined effects of anisotropy, curvature, and non-Darcy resistance in a porous channel. The governing equations are solved using the spectral quasilinearization method, providing a quantitative evaluation of velocity and temperature fields. The results have direct relevance in biomedical applications, such as blood flow through porous tissues, as well as in engineering applications, including heat exchangers, porous media cooling systems, and filtration devices. Additionally, the analysis is applicable to geophysical and energy systems, where anisotropic porous structures significantly influence flow and heat transfer. The study reveals that curvature, anisotropy, and Forchheimer effects substantially modify flow characteristics, leading to reduced velocity and increased temperature —phenomena not captured in earlier models. These findings offer valuable insights for optimising the design and efficiency of systems in both bioengineering and industrial processes.

Novelty and Contributions

- This study investigates fluid flow in a curved porous channel by incorporating the combined effects of anisotropy, curvature, and non-Darcy (Forchheimer) resistance, factors that have rarely been analysed together.
- The governing nonlinear equations are solved using the spectral quasilinearization method (SQLM), which ensures high accuracy and efficiency compared to conventional analytical or numerical approaches.
- The findings demonstrate that curvature and anisotropy substantially alter velocity and temperature distributions, revealing flow and heat-transfer characteristics not captured in earlier models.
- The results provide quantitative insights into velocity reduction and thermal enhancement induced by anisotropy and inertial resistance, with implications for biomedical flows (e.g., blood transport through porous tissues) and engineering systems (e.g., porous heat exchangers, filtration units, and geothermal reservoirs).
- The developed framework establishes a versatile mathematical model that can be extended to non-Newtonian fluids and more complex porous geometries, thereby broadening its applicability to advanced scientific and industrial problems.

2. Formulation of Problem

Modeling Assumptions

1. The flow is steady, incompressible, and hydrodynamically fully developed, which is generated by an azimuthal pressure gradient.
2. The porous domain is homogeneous and anisotropic with directional permeability.
3. Darcy, Brinkman, and Forchheimer effects are all included in the momentum resistance.
4. Thermal equilibrium exists between the fluid and the solid matrix.

This formulation establishes a rigorous mathematical framework for investigating the coupled transport of momentum and thermal energy in Newtonian fluids traversing anisotropic porous curved channels. By systematically incorporating the interplay between anisotropy and curvature-induced modifications to the flow field, the model captures the essential features governing convective transport in confined geometries. Such a formulation is particularly well-suited for advancing the theoretical understanding and design of biomedical transport systems, functional porous membranes, and next-generation microfluidic devices, where precise control of fluid–thermal interactions under anisotropy and curvature is of paramount importance [28]–[31].

Geometry of Problem

We examine a steady, incompressible flow within a curved channel filled with a porous medium which is considered anisotropic. The channel has a diameter of $2H$ and maintains a constant radius of curvature, R (refer to Figure 1). To describe the flow, we employ a curvilinear coordinate system (x, r, z) which is expressed in terms of the Cartesian coordinate system $(X,\ Y,\ Z)$ through the following relationships:

$$X = (R + r)\cos\left(\frac{x}{R}\right), \quad Y = (R + r)\sin\left(\frac{x}{R}\right), \quad Z = z. \tag{2.1}$$

The x coordinate is considered along the channel's centre line, whereas r is normal to it, measured from the channel's centre line. There is no z-direction component, as the flow assumed is two-dimensional. The flow in the channel is produced by a constant pressure gradient $\frac{\partial p}{\partial x} = G$. Let $\bar{\mathbf{V}} = (u, v)$ denote the velocity vector of fluid. As we considered the flow to be fully developed, the x component of velocity u is independent with respect to x and y component velocity v is zero, i.e., $\bar{\mathbf{V}} = (u(r), 0)$.

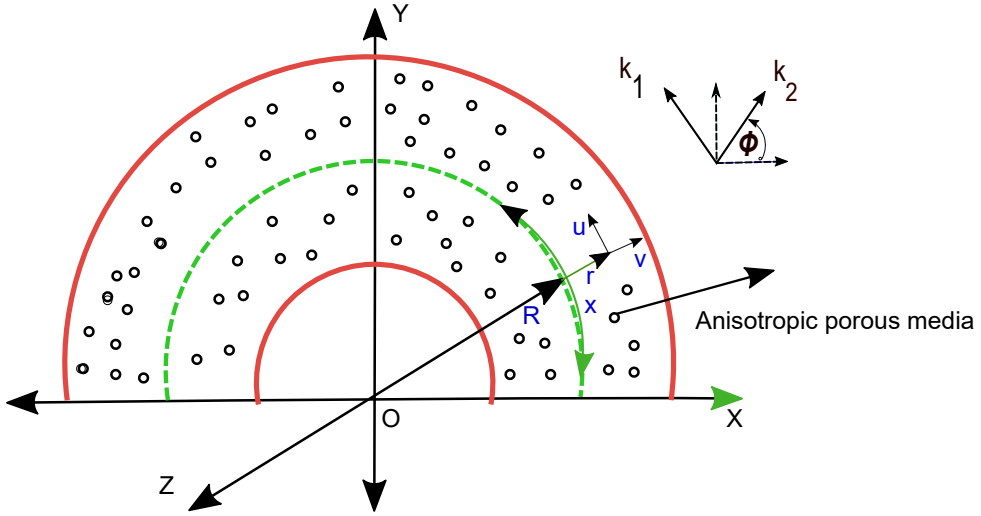

Figure 1: Physical model of problem

In the context of a curved channel with radius R, the governing conservative equations are([12], [14], [32], [33]):

Continuity Equation:

$$\frac{R}{r+R}\frac{\partial u}{\partial x}+\frac{\partial v}{\partial r}+\frac{v}{r+R}=0, \tag{2.2}$$

Momentum Equation:

$$\frac{R}{r+R}\frac{\partial p}{\partial x}-\mu\Big[\frac{d^2u}{dr^2}+\frac{1}{r+R}\frac{du}{dr}-\frac{1}{(r+R)^2}u\Big]+\frac{\mu}{\mathbb{K}}u+\frac{\rho C_F}{\sqrt{\mathbb{K}}}u^2=0, \tag{2.3}$$

Energy Equation:

$$K_f\Big[\frac{d^2T}{dr^2}+\frac{1}{r+R}\frac{dT}{dr}\Big]+\mu\Big(\frac{du}{dr}\Big)^2+\frac{\mu}{\mathbb{K}}f_1u^2+\frac{\rho C_F}{\sqrt{\mathbb{K}}}u^3=0. \tag{2.4}$$

In the above equations, $\mathbb{K}$ denotes the permeability, which is considered a second order tensor in this study due to anisotropy. The anisotropic permeability matrix, and anisotropic angle are described below.

Anisotropic permeability

The anisotropic permeability tensor can be represented as

$$\mathbb{K}=\begin{bmatrix}k_{11} & k_{12}\\ k_{21} & k_{22}\end{bmatrix}. \tag{2.5}$$

k_{ij} represents the components of the permeability tensor. The tensor associated with coefficients of permeability, by reciprocal law, has to be symmetric, i.e., $k_{ij}=k_{ji}$ [see [34]]. In order to analyse the physical properties of material with an anisotropic nature, the on- and off-axis coordinates are commonly used. Figure (2) shows that (x_1x_2) the on-axis represents the primary directions where, for $i\neq j, k_{ij}=0$. Consequently, in an on-axis coordinate system, the components other than diagonal components are zero, and the on-axis permeability tensor is given by:

$$\mathbb{K}_{on}=\begin{bmatrix}k_2 & 0\\ 0 & k_1\end{bmatrix}. \tag{2.6}$$

Off-axis refers to any arbitrary coordinate that deviates -$\phi$from the on-axis coordinate. So we consider the permeability tensor for the off-axis as:

$$\mathbb{K}_{off}=[\mathbf{T}(\phi)]^{-1}\mathbb{K}_{on}[\mathbf{T}(-\phi)]. \tag{2.7}$$

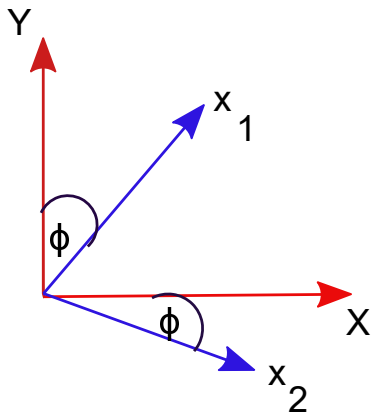

Figure 2: Illustration of on-axis and off-axis coordinate system

where,

$$[\mathbf{T}(\phi)] = \begin{bmatrix} cos\phi & -sin\phi \\ sin\phi & cos\phi \end{bmatrix}. \tag{2.8}$$

By using the property of orthogonality $[\mathbf{T}(\phi)]^{-1}] = [\mathbf{T}(-\phi)]$, for rotational vector we obtain

$$\mathbb{K}_{off} = \mathbf{T}(\phi)\mathbb{K}_{on}\mathbf{T}(-\phi). \tag{2.9}$$

Using equations (2.6), (2.8) in equation (2.9), we get the off-axis permeability tensor components as [see Refs. [35]– [39]]

$$\mathbb{K} = \begin{bmatrix} k_{11} & k_{12} \\ k_{21} & k_{22} \end{bmatrix} = \begin{bmatrix} k_2\ cos^2\phi + k_1\ sin^2\phi & (k_2 - k_1)\ sin\phi\ cos\phi \\ (k_2 - k_1)\ sin\phi\ cos\phi & k_2\ sin^2\phi + k_1\ cos^2\phi \end{bmatrix}. \tag{2.10}$$

Non-Dimensionalization and Boundary Conditions

On considering $\mathbb{K}$, defined in 2.10, in equations 2.11 and 2.12, the momentum and energy equations reduce to:

$$\frac{R}{r+R}\frac{\partial p}{\partial x} - \mu\Big[\frac{d^2u}{dr^2} + \frac{1}{r+R}\frac{du}{dr} - \frac{1}{(r+R)^2}u\Big] + \frac{\mu}{k_1}f_1 u + \frac{\rho C_F}{\sqrt{k_1}}f_2 u^2 = 0, \tag{2.11}$$

$$K_f\Big[\frac{d^2T}{dr^2} + \frac{1}{r+R}\frac{dT}{dr}\Big] + \mu\Big(\frac{du}{dr}\Big)^2 + \frac{\mu}{k_1}f_1 u^2 + \frac{\rho C_F}{\sqrt{k_1}}f_2 u^3 = 0. \tag{2.12}$$

Here, k_1 and k_2 represent vertical and horizontal anisotropic permeability. $K = k_1/k_2$ is the anisotropic permeability ratio and ϕ is the anisotropic angle, the angle formed by positive X axis and horizontal permeability k_2. $f_1 = K\cos^2\phi + \sin^2\phi$, $f_2 = \sqrt{K}\cos^2\phi + \sin^2\phi$ are the parameters characterising the anisotropy. K_f, p, μ, κ, T, and C_F represent thermal conductivity, pressure, viscosity, curvature parameter, temperature and inertial coefficient, respectively. A mathematical description of boundary conditions:

$$u(\pm H) = 0, T(-H) = T_1,\ T(H) = T_2. \tag{2.13}$$

The velocity boundary conditions $u(\pm H) = 0$ represent the no-slip condition at the impermeable channel walls, indicating that the fluid adheres to the surfaces and cannot move along them. The temperature boundary conditions $T(-H) = T_1$, $T(H) = T_2$ impose a constant temperature difference across the channel walls, which establishes a thermal gradient that drives heat transfer. Following are the non-dimensional variables:

$$\tilde{u} = \frac{\mu u}{GH^2},\quad \tilde{r}H = r,\ T = \theta(T_1 - T_2) + T_2,\quad \kappa H = R. \tag{2.14}$$

Using equation (2.14) in equations (2.11), (2.12) and (2.13) we get :

$$-\frac{d^2u}{dr^2}-\frac{1}{(\kappa+r)}\frac{du}{dr}+\Big[\frac{1}{(\kappa+r)^2}+f_1\epsilon^2\Big]u+f_2\epsilon F u^2+\frac{\kappa}{(\kappa+r)}=0, \tag{2.15}$$

$$\frac{d^2\theta}{dr^2}+\frac{1}{(\kappa+r)}\frac{d\theta}{dr}+Br\Big(\frac{du}{dr}\Big)^2+Br\epsilon^2 f_1u^2+Br\epsilon f_2Fu^3=0, \tag{2.16}$$

$$\begin{aligned} u(-1)=0, u(1)=0,\\ \theta(-1)=1, \theta(1)=0, \end{aligned} \tag{2.17}$$

where $Da=\frac{k_1}{H^2}$, $\epsilon^2=\frac{1}{Da}$, $Br=\frac{G^2H^4}{\mu K_f\Delta T}$, $F=\frac{C_F\rho GH^3}{\mu^2}$, $\Delta T=T_1-T_2$.
˜ is dropped here for simplicity.

3. Mathematical Solution

Special case - Isotropic Porous Medium

The analytical solution for the azimuthal velocity is derived only for the isotropic permeability case, where the governing equations are significantly simplified. Its main purpose is to provide theoretical insight and a limiting case for the general anisotropic problem. We consider an isotropic porous media, with permeability K and neglecting the Forchheimer number($F=0$) equation (2.15) becomes

$$\Big[\frac{d^2u}{dr^2}+\frac{1}{r+\kappa}\frac{du}{dr}-\frac{u}{(r+\kappa)^2}\Big]-\frac{u}{Da}=-\frac{\kappa}{r+\kappa}, \tag{3.1}$$

Applying the method of undetermined coefficients, we obtained a solution analytically for the equation (3.1) using the boundary conditions in equation (2.17).

$$u=C_1I_1\left[\frac{\kappa+r}{\sqrt{Da}}\right]+C_2K_1\left[\frac{\kappa+r}{\sqrt{Da}}\right]+\frac{\kappa Da}{\kappa+r}, \tag{3.2}$$

where

$$C_1=\frac{\mathrm{Da}\kappa\left((1-\kappa)K_1\left[\frac{\kappa-1}{\sqrt{\mathrm{Da}}}\right]+(\kappa+1)K_1\left[\frac{\kappa+1}{\sqrt{\mathrm{Da}}}\right]\right)}{(\kappa^2-1)\left(I_1\left[\frac{\kappa+1}{\sqrt{\mathrm{Da}}}\right]K_1\left[\frac{\kappa-1}{\sqrt{\mathrm{Da}}}\right]+I_1\left[\frac{1-\kappa}{\sqrt{\mathrm{Da}}}\right]K_1\left[\frac{\kappa+1}{\sqrt{\mathrm{Da}}}\right]\right)},$$

$$C_2=\frac{\mathrm{Da}\kappa\left((\kappa+1)I_1\left[\frac{\kappa+1}{\sqrt{\mathrm{Da}}}\right]+(\kappa-1)I_1\left[\frac{1-\kappa}{\sqrt{\mathrm{Da}}}\right]\right)}{(\kappa^2-1)\left(I_1\left[\frac{\kappa-1}{\sqrt{\mathrm{Da}}}\right]K_1\left[\frac{\kappa+1}{\sqrt{\mathrm{Da}}}\right]-I_1\left[\frac{\kappa+1}{\sqrt{\mathrm{Da}}}\right]K_1\left[\frac{\kappa-1}{\sqrt{\mathrm{Da}}}\right]\right)}.$$

Here we used I_1 and K_1 the modified first order Bessel functions.

The mean velocity in a curved channel is as follows:

$$\begin{aligned} U=\sqrt{\mathrm{Da}}\Big[-C_1I_0\left[\frac{1-\kappa}{\sqrt{\mathrm{Da}}}\right]+C_1I_0\left[\frac{\kappa+1}{\sqrt{\mathrm{Da}}}\right]+C_2K_0\left[\frac{\kappa-1}{\sqrt{\mathrm{Da}}}\right]\\ -C_2K_0\left[\frac{\kappa+1}{\sqrt{\mathrm{Da}}}\right]\Big]+\mathrm{Da}\kappa\log\left[\frac{\kappa+1}{\kappa-1}\right]. \end{aligned} \tag{3.3}$$

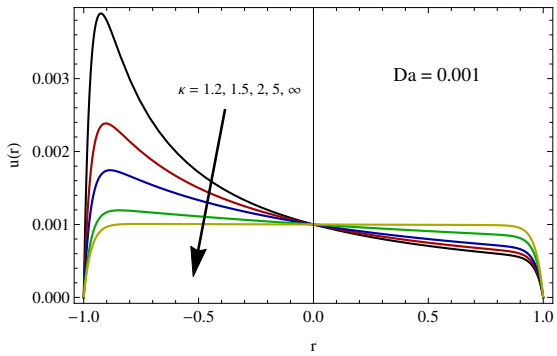

Figure 3: Azimuthal Velocity profiles for different κ.

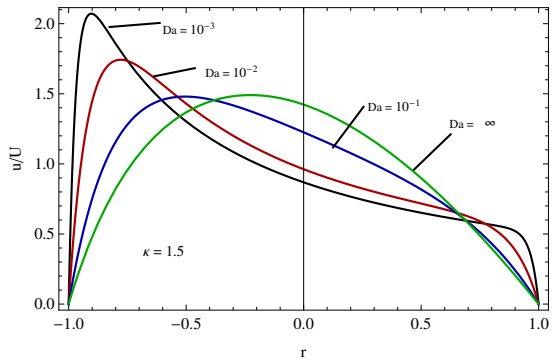

Figure 4: Azimuthal velocity profiles for varying Da in a curved channel.

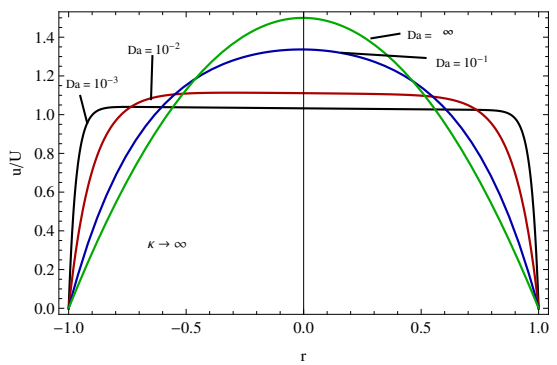

Figure 5: Azimuthal velocity profiles for varying Da in a straight channel.

Numerical Solution - Anisotropic Porous Medium

For the case of anisotropic permeability, the governing equations (2.15) and (2.16), with boundary conditions (2.17), are solved by applying a Spectral Quasilinearization Method (SQLM), which combines the spectral discretization of derivatives with iterative linearization, providing fast convergence and high accuracy for velocity and temperature distributions.

The matrix form of the so-obtained equations is considered as:

$$\begin{bmatrix} \mathbf{A}_{11} & \mathbf{A}_{12} \\ \mathbf{A}_{21} & \mathbf{A}_{22} \end{bmatrix} \quad \begin{bmatrix} \mathbf{u}^{(k+1)} \\ \theta^{(k+1)} \end{bmatrix} = \begin{bmatrix} R_1 \\ R_2 \end{bmatrix}, \tag{3.4}$$

where

$$\mathbf{A}_{11} = -\mathbf{D}^2 - diag\left(\frac{1}{\kappa + r}\right)\mathbf{D} + diag\left[\frac{1}{(\kappa + r)^2} + f_1\epsilon^2 + 2f_2\epsilon F\mathbf{u}^{(k)}\right]\mathbf{I}, \quad \mathbf{A}_{12} = 0,$$

$$\mathbf{A}_{21} = diag(2Br\mathbf{u}'^{(k)})\mathbf{D} + diag(Br\epsilon^2 f_1\ \mathbf{u}^{(k)} + 3Br\epsilon F\ \mathbf{u}^{(k)^2})\mathbf{I}, \quad \mathbf{A}_{22} = \mathbf{D}^2 + diag\left(\frac{1}{\kappa + r}\right)\mathbf{D},$$

$$R_1 = f_2\epsilon F(\mathbf{u}^{(k)})^2 - \frac{\kappa}{\kappa + r}, \quad R_2 = Br(\mathbf{u}'^{(k)})^2 + Brf_1\epsilon^2(\mathbf{u}^{(k)})^2 + Brf_2\epsilon F(\mathbf{u}^{(k)})^3.$$

Here, $\mathbf{u}$, θ are discretised velocity and temperature vectors, and $\mathbf{D}$ denotes the Chebyshev differentiation matrix.

4. Results and Discussions

Special case - Isotropic Porous Medium

In figure (3), we notice a reduction of velocity up to the channel's centre, after which a slight increase as the curvature parameter κ rises. For a fixed κ, we notice maximum velocity near the lower wall for lower Da values in the graph of Figure (4). In curved channels, the pressure gradient drives the flow. A higher Da can reduce the effective pressure gradient available for accelerating fluid in the primary flow direction, leading to a lower velocity. The velocity distribution for a range of Da for fixed κ is shown in Figure (5). This indicates that the fluid's velocity is at its peak at the centre line as it transitions from a curved to a straight channel.

Anisotropic Porous Medium

The influence of parameters, including Forchheimer number, curvature parameter, anisotropic permeability ratio, anisotropic angle, and Darcy number, on fluid flow is investigated. Figures (6) and (7) depict the variations in the velocity profile. In figure 6(a), it is noticed that velocity reduces with a rise in K.

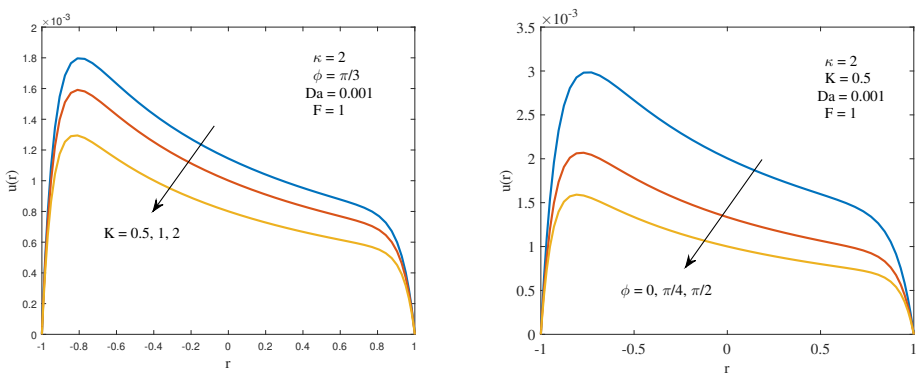

(a) (b)

Figure 6: Velocity profile for varying (a) Anisotropic permeability ratio (b) Anisotropic angle.

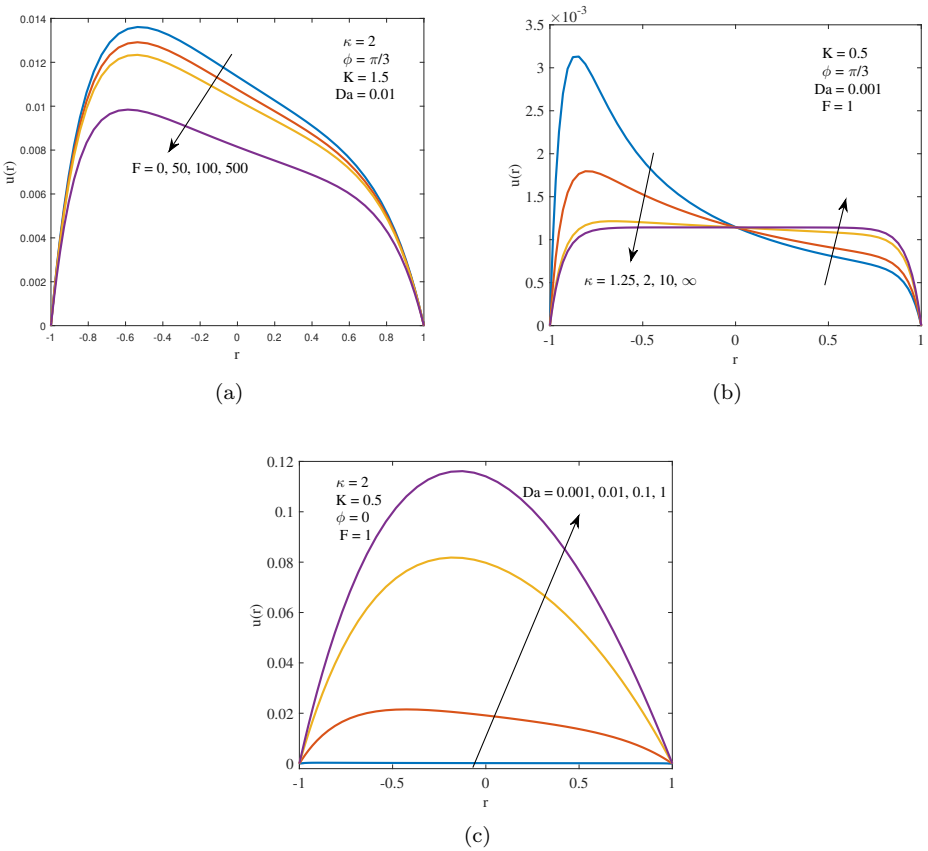

Figure 7: Velocity profile for varying (a) Forchheimer number, (b) Curvature parameter, (c) Darcy number

.

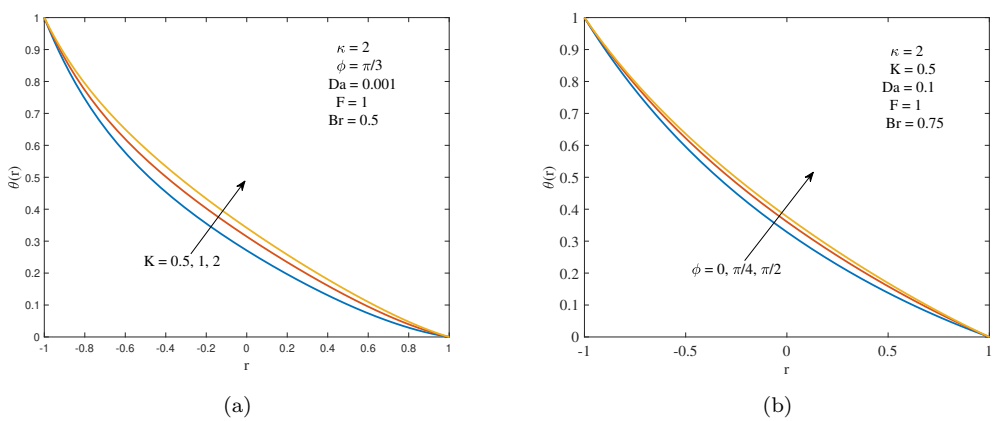

Figure 8: Temperature profile for varying (a) Anisotropic permeability ratio (b) Anisotropic angle.

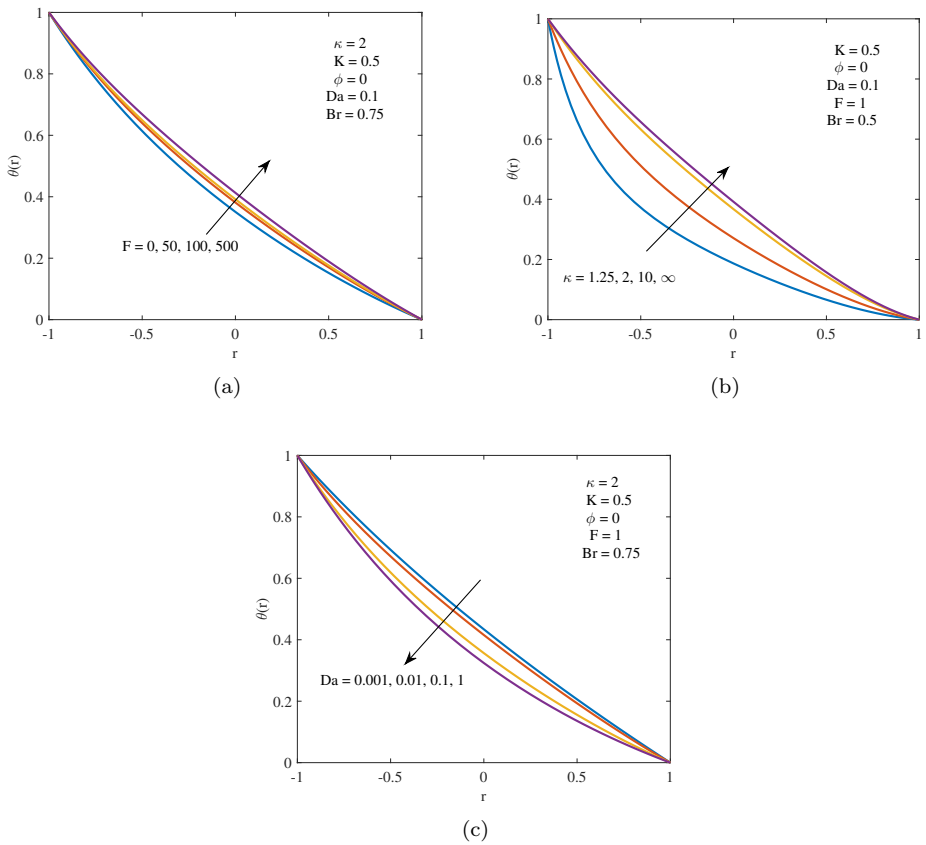

Figure 9: Temperature profile for varying (a) Forchheimer number, (b) Curvature parameter, (c) Darcy number.

The maximum velocity can be noticed closer to the lower wall of the channel. This is consistent with the concept that the value of $K = k_1/k_2$ increases, which implies the horizontal permeability decreases, and so does the velocity. It is observed that relative to the case $K = 0.5$, the peak velocity decreases by about 17% when $K = 0.1$ and by approximately 33% when $K = 2$. Figure 6(b) depicts the variation of velocity with an anisotropic angle. Optimal velocity is attained when $\phi = 0$, while the lowest velocity is seen when $\phi = \frac{\pi}{2}$. This behaviour is consistent with the concept that when the value of K is less than 1 and keeping Da or k_1 constant, the value of $\phi = 0$ is equivalent to k_2, the horizontal permeability, which results in a reduction in permeability along the flow direction. Conversely, if $K > 1$, the behaviour will be the opposite. Figure 7(a) illustrates the effect of the Forchheimer number F on the velocity profile. As F increases, the inertial resistance within the porous medium grows, which opposes the flow and leads to a reduction in velocity. This trend highlights the significance of non-Darcy (Forchheimer) effects in controlling the fluid motion through the porous channel. Figure 7(b) illustrates the velocity profile across the channel. As the curvature parameter κ increases, the velocity decreases toward the channel centre, after which it rises, indicating that the optimal velocity occurs near the inner wall of the curved channel. The optimal velocity is noticed close to the curved channel's inner wall. Notably, as the channel transitions from a highly curved state ($\kappa = 1.25$) to a straight state ($\kappa = \infty$), the peak velocity is reduced by nearly 70%. This significant reduction is a quantitative measure of the diminishing effect of centrifugal forces, which are prominent in curved channels and contribute to higher, asymmetric velocity profiles. An increasing profile of velocity for various Da values is illustrated in Figure 7(c). A higher Da signifies a higher permeability and hence the increase in velocity. The optimal velocity is noticed close to the middle of the channel. Figures (8) and (9) illustrate the profiles of temperature for

various parameters. We can observe that an increase of K enhances the temperature. This is consistent with the idea that Nu rises with a rise in anisotropic ratio, leading to improved heat transmission and, eventually, temperature (see 8(a)). The graph in 8(b) depicts an increase in temperature as ϕ increases. As ϕ increases, the alignment of the permeability direction becomes increasingly unfavourable for fluid flow. This misalignment increases resistance to fluid movement, necessitating greater effort for the fluid to traverse the medium. The augmented resistance produces friction, resulting in heat generation and an increase in temperature. A rise in temperature has been noticed with an increase in Forchheimer number F (see figure 9(a)). When we increase F, the inertial drag effects cause increased energy dissipation and also prolonged heat transfer due to increased resistance and reduced velocity. In Figure 9(b), we notice a rise in temperature with a rise in curvature parameter. In curved channels, centrifugal forces are generated, which lead to the development of secondary flows. These stronger centrifugal forces cause flow separation and lead to heat accumulation, which causes a rise in temperature. The central temperature is observed to increase by approximately 16% as the channel transitions from a highly curved state ($\kappa = 1.25$) to a straight configuration ($\kappa \to \infty$). Figure 9(c) illustrates the decrease in temperature with an increase of Da. As Da increases, the flow velocity increases, and heat transfer becomes more efficient in carrying the heat away and thereby reducing the temperature. The velocity decay near the outer wall and the increase in temperature with curvature are consistent with the reports in literature [14,23].

5. Conclusions

This work has investigated the combined influence of anisotropy, Darcy number, Forchheimer effects, and curvature on fluid flow and heat transfer in a porous channel. To create graphs that illustrated the effects of some significant physical parameters found in the review, an internal MATLAB program was utilised. Based on the obtained velocity and temperature distributions, the following key findings are noted:

- Rising values of anisotropic permeability ratio K, anisotropic angle ϕ, and Forchheimer number F, the magnitude of velocity decreases and temperature increases.
- Relative to $K = 0.5$, the peak velocity decreases by about 17% when $K = 0.1$ and by approximately 33% when $K = 2$. A rise in K from 0.5 to 1 results in an increase of nearly 14% in the central channel temperature, and increasing K to 2 further elevates the temperature by approximately 28% compared to the baseline ($K = 0.5$).
- A Higher Darcy number Da results in a rise in velocity and a reduction of temperature.
- With an increase of curvature parameter κ, an increase in temperature is observed and a reduction of velocity till the centre while increasing moving towards the outer curve.
- As the channel transitions from a highly curved state ($\kappa = 1.25$) to a straight state ($\kappa = \infty$), the peak velocity is reduced by nearly 70%. This significant reduction is a quantitative measure of the diminishing effect of centrifugal forces, which are prominent in curved channels and contribute to higher, asymmetric velocity profiles. The central temperature rises by approximately 16% as the channel transitions from a highly curved state ($\kappa = 1.25$) to a straight configuration ($\kappa \to \infty$).

Unlike previous isotropic models, this study provides a quantitative evaluation of anisotropic permeability ratio and anisotropic angle together with non-Darcy flow effects, showing how their interplay governs both the velocity field and the temperature distribution. These findings establish how anisotropy, inertial resistance, and curvature interact in curved porous channels, providing a novel quantitative characterisation of their competing effects. The results offer useful predictive guidelines for optimising biomedical devices, porous flow systems, and curved heat exchangers. This research aims to bridge theoretical understanding and practical utility in diverse technological and scientific domains.

Limitations and Future scope

This study is limited by the assumptions of steady, fully developed flow, homogeneous anisotropic porous medium, and local thermal equilibrium. Future work may address unsteady effects and additional forces, such as magnetic fields or non-Newtonian fluids, to broaden the applicability of the model.

References

1. Goldstein, S., *Modern Developments in Fluid Dynamics: An Account of Theory and Experiment Relating to Boundary Layers, Turbulent Motion and Wakes*, Vol. 2, Clarendon Press, Oxford (1938).
2. So, R. M., *Entry flow in curved channels*, J. Fluid Mech., 98(2), 305–310 (1976).
3. Abdalbagi, M., *Micropolar flow and heat transfer within a permeable channel using the successive linearization method*, Open Physics, 21(1), (2023). doi: 10.1515/phys-2023-0177.
4. Ahmad, S., Ashraf, M., Ali, K., and Nisar, K., *Computational analysis of heat and mass transfer in a micropolar fluid flow through a porous medium between permeable channel walls*, Int. J. Nonlinear Sci. Numer. Simul., 23(5), 761–775, (2022). doi: 10.1515/ijnsns-2020-0017.
5. Alharbey, R., Mondal, H., and Behl, R., *Spectral quasi-linearization method for non-Darcy porous medium with convective boundary condition*, Entropy, 21, 838, (2019). doi: 10.3390/e21090838.
6. Boodoo, C., *Micropolar fluid flows past a porous shell: A model for drug delivery using porous microspheres*, Eur. J. Eng. Technol. Res., 9(3), 1–7, (2024). doi: 10.24018/ejeng.2024.9.3.3162.
7. Chaithra, N., and Hanumagowda, B. N., *Effect of micropolar fluid to study the characteristics of squeeze film between porous curved annular plates*, Communications in Mathematics and Applications, 14(4), 1469–1478, (2023).
8. Humane, P., Patil, V., Patil, A., and Shamshuddin, D. M., *Buongiorno modelled nanoliquid consequence of thermal and solutal convection on the magneto-micropolar fluid inside an inclined porous stretching device*, Journal of Nanofluids, 12, 211–222, (2023). doi: 10.1166/jon.2023.1949.
9. Ishaq, M., Rehman, S. U., Riaz, M. B., and Zahid, M., *Hydrodynamical study of couple stress fluid flow in a linearly permeable rectangular channel subject to Darcy porous medium and no-slip boundary conditions*, Alexandria Engineering Journal, 91, 50–69, (2024). doi: 10.1016/j.aej.2024.01.066.
10. Jalili, B., Azar, A. A., Jalili, P., and Ganji, D. D., *Analytical approach for micropolar fluid flow in a channel with porous walls*, Alexandria Engineering Journal, 79, 196–226, (2023). doi: 10.1016/j.aej.2023.08.015.
11. Berman, A.S., *Laminar flow in channels with porous walls*, J. Appl. Phys., Vol. 24, pp. 1232–1235 (1953).
12. Kuznetsov, A., Avramenko, A., *Flow in a curved porous channel with a rectangular cross section*, J. Porous Media 11, 241–246, (2007).
13. Okechi, N. F., Asghar, S., *Fluid motion in a corrugated curved channel*, Eur. Phys. J. Plus 134, (2019).
14. Yadav, P. K., Yadav, N., *A study on the flow of couple stress fluid in a porous curved channel*, Comput. Math. Appl. 152, 1–15, (2023).
15. Sharma, S., Sharma, K., *Unsteady flow of couple stress fluid through an anisotropic porous medium with time-dependent boundary conditions*, J. Porous Media 22, 837–850, (2019).
16. Jaiswal, S., Yadav, P., *Physics of generalized couette flow of immiscible fluids in anisotropic porous medium*, Int. J. Mod. Phys. B 38, (2023).
17. Maiti, S., Das, S., *Numerical analysis of couple stress fluid flow in an anisotropic porous medium with heat generation*, Int. J. Numer. Methods Heat Fluid Flow 30, 28–45, (2020).
18. Prakash, V., Nanda, S., *Hydrodynamic flow of couple stress fluid through an anisotropic porous medium with suction and injection*, Appl. Math. Model. 79, 501–516, (2020).
19. Vijaya Sree, R., Narla, V. K., *Impact of anisotropic permeability on micropolar fluid dynamics and heat transfer in porous channels*, East Eur. J. Phys. 4, 107–121, (2024). doi:10.26565/2312-4334-2024-4-10
20. Vijaya Sree, R., Narla, V. K., Babu, K. S., *A biomagnetic couple stress fluid flow in an anisotropic porous channel with stretching walls*, East Eur. J. Phys. 4, 159–176, (2024). doi:10.26565/2312-4334-2024-4-15
21. Karmakar, T., Raja Sekhar, G., *Effect of anisotropic permeability on fluid flow through composite porous channel*, J. Eng. Math. 100, 33–51, (2016).
22. Karmakar, T., Raja Sekhar, G. P., *A note on flow reversal in a wavy channel filled with anisotropic porous material*, Proc. R. Soc. A: Math. Phys. Eng. Sci. 473, 20170193, (2017).
23. Nakayama, A., Kuwahara, F., Umemoto, T., Hayashi, T., *Heat and fluid flow within an anisotropic porous medium*, J. Heat Transfer 124, 746–753, (2002).
24. Pandey, A.K., Gupta, T., *Mixed convective flow of Ag–H_2O magnetic nanofluid over a curved surface with volumetric heat generation and temperature-dependent viscosity*, Heat Transfer Engineering, 42(24), 2204685, (2021). doi:10.1002/htj.22227
25. Bartwal, P., Pandey, A.K., Upreti, H., *Impact of anisotropic slip on magnetized tangent hyperbolic fluid flow over a rotating disk: A Legendre wavelet collocation method*, International Communications in Heat and Mass Transfer, 159, 108081, (2024). doi:10.1016/j.iche.2024.108081
26. Upreti, H., Pandey, A., Kumar, M., Makinde, O.D., *Darcy–Forchheimer flow of CNTs–H_2O nanofluid over a porous stretchable surface with Xue model*, International Journal of Modern Physics B, 37(5), 2350018, (2023). doi:10.1142/S0217979223500182

27. Prakash, J., *Melting heat transfer and irreversibility analysis in Darcy–Forchheimer flow of Casson fluid modulated by EMHD over cone and wedge surfaces*, Journal of Thermal Analysis and Calorimetry, 145(2), 1065–1077, (2024). doi:10.1007/s10973-024-12085-4

28. Aich, R., *Impact of heat transfer in a duct composed of anisotropic porous media*, Int. J. Heat Mass Transf. 173, 121302, (2024). doi:10.1016/j.ijheatmasstransfer.2021.121302.

29. Barletta, A., *Linearly unstable forced and free flow in an anisotropic porous medium*, Int. J. Heat Mass Transf. 173, 121302, (2024). doi:10.1016/j.ijheatmasstransfer.2024.121302.

30. Mudugamuwa, A., *Periodic flows in microfluidics*, Small 20(24), 2204685, (2024). doi:10.1002/smll.202404685.

31. Guo, W., *Effect of pore-scale anisotropic and heterogeneous structures on gas flow in porous media*, Materials 10(7), 175, (2025).

32. Avramenko, A.A. and Kuznetsov, A.V., *Instability of a slip flow in a curved channel formed by two concentric cylindrical surfaces*, European Journal of Mechanics B/Fluids 28(6), 722–727, (2009). doi:10.1016/j.euromechflu.2009.06.003.

33. Karmakar, T., Reza, M., Raja Sekhar, G. P., *Forced convection in a fluid saturated anisotropic porous channel with isoflux boundaries*, Phys. Fluids 31, 117109, (2019).

34. Norouzi, M., Shoghi, M. R., *A numerical study on miscible viscous fingering instability in anisotropic porous media*, Phys. Fluids 26, 084102, (2014). doi:10.1063/1.4891228.

35. Karmakar, M. R. T., Alam, M., Raja Sekhar, G. P., *Couette-Poiseuille flow in a fluid overlying an anisotropic porous layer*, Comput. Math. Appl. 151, 346–358, (2023).

36. Ghosh, N., Karmakar, T., Raja Sekhar, G. P., *Application of conformal mapping to two-dimensional flows in an anisotropic aquifer*, Indian J. Pure Appl. Math. 53, 617–626, (2022).

37. Karmakar, T., Raja Sekhar, G. P., *Squeeze-film flow between a flat impermeable bearing and an anisotropic porous bed*, Phys. Fluids 30, 043604, (2018).

38. Pramanik, S., Karmakar, T., *Couette-Poiseuille flow of variable viscosity in a multilayered channel partially filled with a homogeneous anisotropic porous layer: Role of the glycocalyx in attenuating shear stress on endothelial cells*, Phys. Fluids 36, 033615, (2024).

39. Rees, L. S. D. A. S., Postelnicu, A., *The onset of convection in an inclined anisotropic porous layer with oblique principal axes*, Transp. Porous Media 62, 139–156, (2006).

V. K. Narla,
Department of Mathematics,
GITAM Deemed to be University, Hyderabad,
India.
E-mail address: vnarla@gitam.edu

and

R. Vijaya Sree,
Department of Mathematics,
ACE Engineering College, Hyderabad,
India.
E-mail address: rv.jayasree@gmail.com

and

K. Suresh Babu,
Department of Mathematics,
Gokaraju Rangaraju Institute of Engineering & Technology, Hyderabad,
India
E-mail address: suresh.tammala@gmail.com